Journal of ELECTRONIC MATERIALS, Vol. 50, No. 4, 2021
https://doi.org/10.1007/s11664-020-08534-8

ASIAN CONSORTIUM ACCMS–INTERNATIONAL CONFERENCE ICMG 2020

Influence of ZnO Doping on Spectral Properties of Sol–Gel Derived CdO–$FePO_4$ Nanocomposites

S.K. KHAJA MUSWAREEN[1] and SANDHYA COLE[1,2]

1.—Department of Physics, Acharya Nagarjuna University, Nagarjuna Nagar, Guntur, A.P. 522510, India. 2.—e-mail: sandhya.cole@gmail.com

The focus of this study are the spectral properties of undoped and zinc oxide (ZnO) doped cadmium oxide iron phosphate (CdO–$FePO_4$) nanocomposites synthesized through a sol-gel approach. Doping of ZnO into the CdO–$FePO_4$ matrix is confirmed through various spectroscopic techniques at room temperature for 0.3 mol.%, 0.6 mol.%, and 0.9 mol.% of ZnO concentration. X-ray diffraction (XRD) pattern indicates that prepared CdO–$FePO_4$ nanocomposites doped with ZnO correspond to the cubic crystalline nature of CdO, hexagonal amorphous nature of $FePO_4$ and tend to form nanometer size of about 21 nm. The morphological analysis of the produced nanocomposites is done via scanning electron microscopy and transmission electron microscopy (TEM) images. The particle sizes found from TEM images are in the nanometer regime and are in good agreement with the results obtained from XRD. The functional groups corresponding to CdO bands and PO_4 groups are observed for the prepared samples from Fourier transform infrared (FT-IR) and Raman spectra. The optical bandgaps of CdO–$FePO_4$ nanocomposites doped with ZnO are deduced by diffused reflectance measurements. The photoluminescence spectrum exhibits bands in the visible range signifying the quantum confinement-induced photoluminescence, and the resultant CIE coordinates and CCT values are explored in search of their applicability in home appliances.

Key words: ZnO, CdO, $FePO_4$, sol–gel method, cubic, hexagonal

INTRODUCTION

One of the essential goals of materials research is to expand ways of attaining materials with distinct applications based on their peculiar properties.[1] Nanomaterials have revealed intense interest during recent years due to their remarkable chemical and physical properties that differ considerably from the bulk form of the same materials. Furthermore, nanoscale semiconductors permit greater absorption of photons, thereby improving the system efficiency and resulting in novel developments in various fields of nanotechnology.[2] In the current work, the significance, synthesis, and characterization of semiconducting CdO–$FePO_4$ nanocomposites with ZnO for advanced technological applications are discussed. Cadmium Oxide (CdO) in nanocrystalline form is an important n-type metal oxide semiconductor with a direct and indirect bandgap of 2.2–2.7 eV and 1.36–1.98 eV, respectively.[3] The bandgap value also depends on the preparation conditions. CdO nanomaterials and metal-doped CdO nanomaterials have a broad range of optoelectronic applications such as flat panel displays, optical communications, photo-diodes, photo-transistors, smart windows, solar-cells, transparent electrodes, and transparent conducting oxide (TCO). CdO is also used in different types of applications such as IR heat mirrors, gas sensors, low-emissive windows, and thin-film resistors.[3,4]

(Received March 17, 2020; accepted September 26, 2020; published online October 21, 2020)

Particularly, CdO shows potential applications in solar cells owing to its high optical transmittance in the visible range of solar spectrum and high electrical conductivity.[4] In recent times, metal-based nanostructured materials in an oxide matrix are broadly analyzed for diverse applications on account of their novel physiochemical properties. Moreover, the ferrites substituted in cadmium act as n-type semiconductors, and the increase of cadmium content results in a gradual decrease of the Seebeck coefficient. Typically, cadmium-iron (Cd-Fe)-based complex oxides exhibit selectively high sensitivity to ethanol gas over hydrogen, isobutene, and carbon monoxide.[5,6] Also, metal phosphates are of immense interest in catalytic applications because of their desirable properties such as acid stability, catalytic activity, high proton conductivity, and open framework structures.[7] Among various phosphate-based materials, iron phosphate ($FePO_4$) is a white, weakly soluble Fe compound of slight nutritional value caused by its low bioavailability.[8] In general, $FePO_4$ may be considered a charge-transfer insulator with a wide bandgap energy of $\sim$ 4 eV.[9,10] Although $FePO_4$ has low electrical conductivity, enhancing the properties of stability, cost-effectiveness and low-toxicity attempts are made to advance the performance as cathode material for rechargeable batteries.[11] Further, it is also essential to prepare and examine the nanostructured electrodes for their prospective use in fuel cells, since their performance depends not only on the characteristics of the phosphate matrix but also on the composite nanostructures of metal nanophase. Also, there have been many research attempts to design hybrid nanostructures of $FePO_4$ upon substitution of supporting matrices or by coating conductive materials such as metal oxides, metals, and polymers using diverse synthetic routes to improve the conductivity of $FePO_4$.[12,13] In this study, we have synthesized CdO–$FePO_4$ nanocomposite for its possible use in various potential applications (viz., as cathode material in rechargeable batteries, photo-catalysis). The applications of synthesized nanocomposites can be improved via a process of doping with diverse metallic ions.[4]

In general, transition metal oxides are used to dope the nanocomposites because their outermost d-orbitals are incompletely filled and can easily receive or donate electrons. Aydin[4] studied the structural and optical properties of Fe-doped CdO nanopowders prepared by the sol–gel approach. Until now, this type of work has not been done, i.e., on the synthesis of CdO–$FePO_4$ nanocomposites doped with zinc oxide (ZnO) by sol–gel method. In this study, ZnO doped CdO–$FePO_4$ nanocomposites are reported and the doping effects are investigated. ZnO is an n-type semiconducting material exhibiting piezoelectric or pyroelectric properties and hence can be used in many devices and electrochemical applications.[2] Nanostructured ZnO is broadly used as an ideal material in both low-level and high-level thermo-optical-electronic device circuits that can be operated reasonably in rigid environments.[14] ZnO-based energy systems have received much interest in research and development since the beginning of the nineteenth century. Advantages related to zinc-based systems are low-cost, low-toxicity, and highly stable.[15] Also, ZnO-based batteries maintains a huge production to meet the increasing demand for electric propulsion.[16] Hence, considering the unique optoelectronic properties and diverse applications of ZnO, it is interesting to study the influence of ZnO doping on the CdO–$FePO_4$ nanocomposite.

The synthesis technique has a considerable impact on the properties of nanocomposites, and these properties have a significant impact on the applications of nanocomposites. The control size and morphology of the nanocomposites can also be achieved by choosing a suitable synthetic route. In general, the citric acid gel method, combustion synthesis, co-precipitation, hydrothermal method, sol–gel, and solid-state reaction have been developed to synthesize the nanocomposite materials.[17] Among these different synthetic routes, sol–gel is a sensible synthetic approach to attain high-quality nanopowders for various technological applications.[4] Thus, CdO–$FePO_4$ nanocomposites doped with ZnO are synthesized by means of the sol–gel process and the structural, optical, and magnetic properties are investigated in the present work.

EXPERIMENTAL

Synthesis of Nanocomposites

Cadmium oxide (CdO), iron phosphate ($FePO_4$), and zinc oxide (ZnO) of high purity, i.e., 99.9% analar grade, are used as the starting materials for the synthesis of the undoped and ZnO doped CdO–$FePO_4$ nanocomposites via sol–gel route. According to the desired stoichiometry, the chemicals were weighed and dissolved in deionized 240 ml of water and ethanol in a beaker. The resulting solution was stirred constantly using a magnetic stirrer at room temperature, and then an equal molar measure of sodium hydroxide (NaOH) solution in a deionized water-ethanol matrix was added dropwise to the mixture under constant stirring for 8 h touching the walls of the beaker until an aqueous solution was attained. The formation of the CdO–$FePO_4$ nanocomposite was evidenced by the formation of a yellowish-brown colloid. To eliminate impurities, the solution was washed numerous times with deionized water and the collection of precipitates is done via centrifugation process. Further, the annealing chamber operating at ambient pressure is used to dry the collected precipitates at 200°C for 2 h. Thus, the CdO–$FePO_4$ nanocomposites doped with ZnO (0.3 mol.%, 0.6 mol.%, and 0.9 mol.%) are prepared.

Characterization Techniques

Various characterization techniques were employed to examine CdO–$FePO_4$ nanocomposites doped with ZnO. Crystallinity of the prepared samples in 10°–80° (2θ) scanning range were measured by an x-ray diffractometer (Philips: PW1830) with a wavelength of CuKα radiation (1.5406 Å) at 2 °/min scanning rate upon maintaining the current and operating voltage at 30 mA and 40 kV, respectively. The morphology and energy dispersive x-ray diffraction spectroscopy (EDAX) were acquired from an S-3400: Scanning electron microscope, with an accelerating voltage of 10 kV. TEM images of the nanocomposites were obtained from a Hitachi HT7700 microscope operated at 100 kV. A Fourier transform infrared spectrometer (Perkin Elmer Spectrum1: FT-IR Spectrometer) was used to acquire FT-IR spectra of KBr mixed synthesized nanocomposites in the scanning range 4000–450 cm^{-1}. Raman spectra of the prepared nanocomposites were recorded by the FT-Raman spectrometer (BRUKER RFS 27) in the 4500–50 cm^{-1} spectral range. A UV-Vis-NIR spectrophotometer (Perkin Elmer Lambda 950) was used to obtain UV-Vis spectra of prepared samples mixed with Nujol (liquid paraffin) within the wavelength range of 200–1200 nm. A Lambda 900 UV/VIS/NIR spectrophotometer with an attached integrating sphere was used to record the diffused reflectance spectra of the synthesized samples within the wavelength region of 200–2500 nm. A PERKIN ELMER LS-55 with a xenon lamp excited at 350 nm as a source was used to record the PL spectrum. A JEOL JES-FA200 instrument, operating with X-band frequency (8.75–9.65 GHz), 7 × 10^9 spins/0.1 mT sensitivity, and a resolution of 2.35 μT or better was used to record the room-temperature electron paramagnetic resonance (EPR) spectra.

RESULTS AND DISCUSSION

Powder XRD Study

The XRD patterns of undoped and CdO–$FePO_4$ nanocomposites doped with ZnO are presented in Fig. 1. XRD analyses confirm the existence of nanocrystalline CdO and amorphous $FePO_4$ in the CdO–$FePO_4$ nanocomposites.[7,18,19] All the sharp diffraction intensities correspond to the cubic phase of CdO. Diffraction patterns corresponding to the hexagonal phase of $FePO_4$ are not noted showing that $FePO_4$ is most likely to be amorphous at the preferred annealing temperature (200°C).[20] No more impurity diffraction peaks are detected. The strong diffraction peaks attained in all the produced nanocomposites at 2θ values ≈ 33.01°, 38.38°, 55.34°, 65.93° and 69.38° related to the lattice planes (111), (200), (220), (311), (222), respectively, confirm that the prepared nanocomposites correspond to the crystallographic phase of the cubic structure of CdO and match with the standard

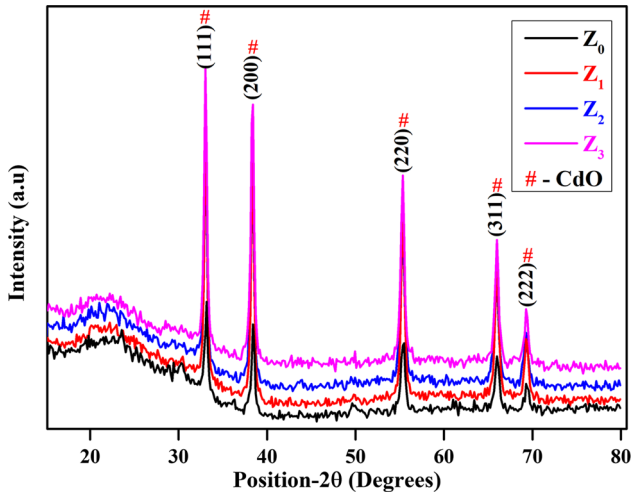

Fig 1. XRD pattern of CdO–$FePO_4$ nanocomposites doped with ZnO.

JCPDS No: 05–0640. The prominent diffraction peak is the (111) plane related preferred orientation. It is also noteworthy that the foremost diffraction peaks become sharper and stronger by increasing the dopant ion concentration, indicating improved crystallinity of the CdO–$FePO_4$ nanocomposites. The lattice cell parameters corresponding to undoped and CdO–$FePO_4$ nanocomposites doped with ZnO show a slight difference in their values, although the structures are identical indicating the substitution of ZnO ions in the CdO–$FePO_4$ lattice site. The evaluated values of cell parameters of the lattice with corresponding unit cell volume and symmetry axes for undoped and CdO–$FePO_4$ nanocomposites doped with ZnO are given in Table I.

The average crystallite size (D) of as-synthesized CdO–$FePO_4$ nanocomposites doped with ZnO are calculated from Debye-Scherrer's relation,[21]

$$D = \frac{0.89\lambda}{\beta \cos\theta} \tag{1}$$

The lattice strain (ε) induced in the nanocomposites is also considered from the Stokes-Wilson relation,[22]

$$\varepsilon = \frac{\beta}{4 \tan\theta} \tag{2}$$

where λ is the incident x-ray wavelength (1.5406 Å), β is high-intensity diffraction peak full width at half maximum (FWHM) in radians and θ is Bragg's diffraction angle.

The dislocation density (δ) is approximated from the crystallite size (D) value[23] using the Williamson-Smallman equation,

$$\delta = 1/D^2 \tag{3}$$

The resultant values of D, ε, and δ for undoped and CdO–$FePO_4$ nanocomposites doped with ZnO are deliberate in Table II. The substitution of zinc ions in the CdO–$FePO_4$ lattice site is shown by the slight difference in lattice cell parameters as in Table I. From Table II, it is seen that lattice strain decreases as the crystallite size increases. Also, dislocation density depends purely on the D value of the as-synthesized samples. From Table II it is found that the sample with 0.9 mol.% of ZnO has the lowest value of 20.22 nm signifying that it has a larger surface area compared with other samples.

Morphological Studies (SEM with EDAX and TEM)

SEM is a vital technique to study the morphology, topography, composition, and distribution of particles in the sample. Figure 2 demonstrates the SEM images of undoped and CdO–$FePO_4$ nanocomposites doped with ZnO. The SEM images of the prepared sample exhibit spherical like agglomerations with some rod-like structures for undoped CdO–$FePO_4$ nanocomposite. It is been observed that by increasing the ZnO concentration (i.e., 0.3, 0.6 mol.%) the spherical agglomerations form a network with rod-like structures. Further, the increase in the concentration of ZnO (i.e., 0.9 mol.%) leads to an increase of rod-like structures forming a network with few spherical agglomerations. This indicates that the doping of ZnO has a strong influence on the morphology of CdO–$FePO_4$ nanocomposites.

The elemental compositions of the prepared nanocomposites are further studied by the EDAX spectrum. The EDAX spectra of undoped and CdO–$FePO_4$ nanocomposites doped with ZnO are presented in Fig. 3. The spectra indicate the presence of Cd, Fe, P, O, and Zn species in the nanocomposites and the elemental composition of undoped and 0.3 mol.%, 0.6 mol.%, 0.9 mol.% of ZnO doped CdO–$FePO_4$ nanocomposites indexed in the table in Fig. 3 which is in good agreement to the chosen stoichiometric ratio. It has also been noticed from the compositional analysis that upon an increase of ZnO doping concentration from 0.3–0.9 mol.% the Zn content increases, indicating the substitution of Zn ions with other ions of the host lattice. Thus, it is clear that doping of ZnO has a strong influence on the host lattice structure. Also, from EDAX spectra, it is clear that our host lattice contains mostly light and intermediate elements (since only the K and L series of x-rays are emitted).

The TEM micrographs shown in Fig. 4 demonstrate the shapes of CdO–$FePO_4$ nanocomposites doped with ZnO. They formed spherical agglomerates and rods of various diameters. Interestingly, there is an immense variation in morphology with an increase in ZnO concentration in accordance with the results obtained from SEM. The particle size distributions relating to the measured diameters of spheres and measured widths of rods from TEM micrographs for all synthesized nanocomposites are presented in Figs. 5 and 6, respectively. From the comparative analysis of Figs. 5 and 6 it has been noted that although the size of the particle

Table I. Lattice cell parameters, unit cell volume and axes of symmetry for CdO–$FePO_4$ nanocomposites doped with ZnO

	CdO		
Sample Code	**Lattice cell parameters (Å) $A = b = c$**	**Unit cell volume V $(Å)^3$**	**Axes of symmetry $\alpha = \beta = \gamma$**
Z_0	4.691	103.210	90°
Z_1	4.692	103.354	90°
Z_2	4.690	103.210	90°
Z_3	4.692	103.344	90°

Table II. Average crystallite size, strain and dislocation density for CdO–$FePO_4$ nanocomposites doped with ZnO

Sample Code	Position (2θ)	FWHM (β)	Crystallite size (d) (nm)	Lattice strain [(ε) × 10^{-4}]	Dislocation density (δ) (lines/m^2)
Z_0	33.02	0.4019	20.39	59.13	2.40×10^{15}
Z_1	32.97	0.3798	21.57	55.98	2.14×10^{15}
Z_2	33.01	0.3977	20.60	58.53	2.35×10^{15}
Z_3	33.13	0.4055	20.22	59.45	2.44×10^{15}

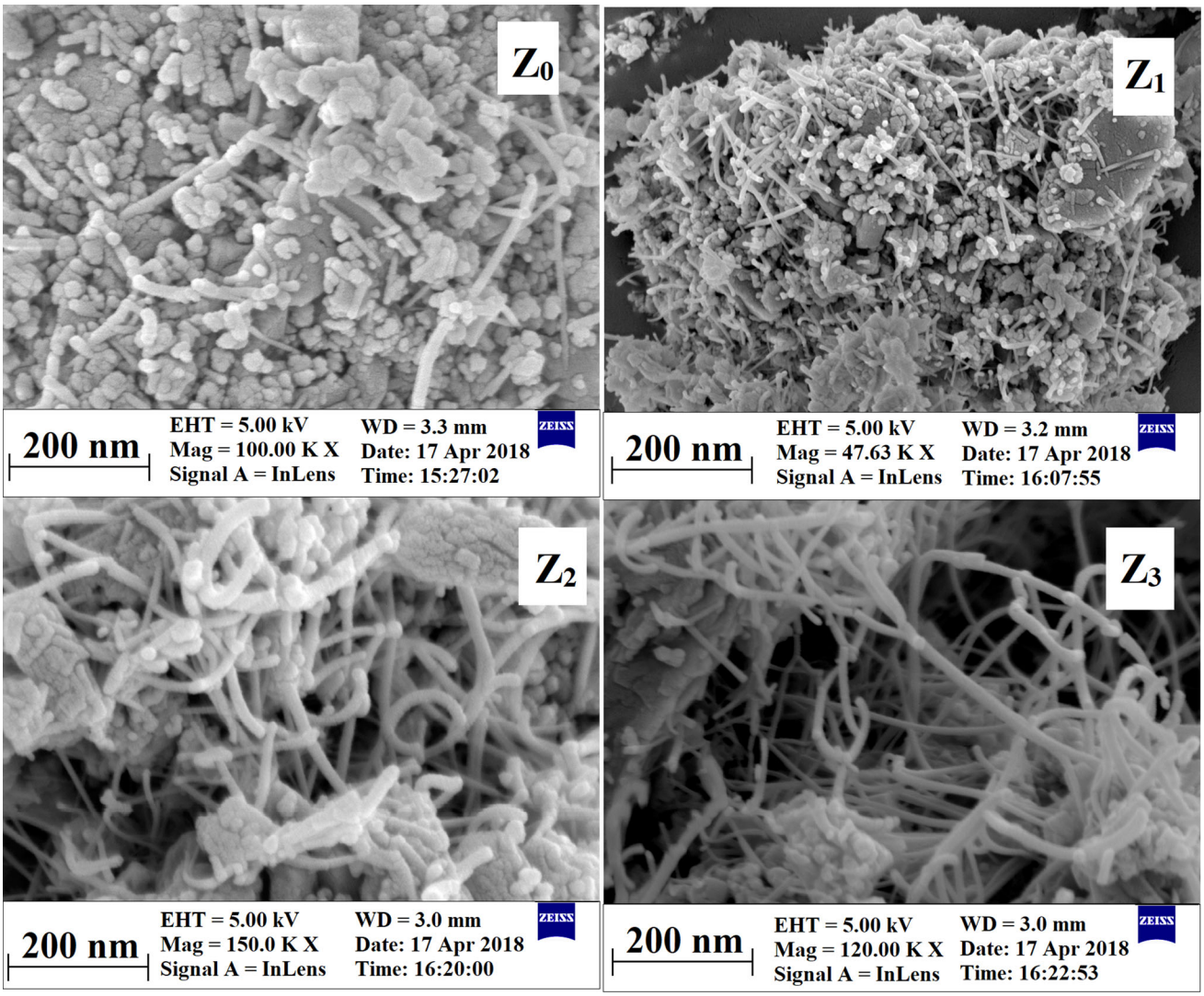

Fig 2. SEM images of CdO–$FePO_4$ nanocomposites doped with ZnO.

is not uniform, most of the spherical agglomerates have dimensions between 15 and 30 nm and most of the rods have dimensions between 10 and 20 nm.

In addition, the particle size of both spherical agglomerates and rods structures for CdO–$FePO_4$ nanocomposites doped with ZnO given in Table III are evaluated from the solid line represented in all particle size distribution graphs which correspond to the log-normal distribution fit. The particle sizes of spherical agglomerates and rods varied between 21.04 and 24.70 and 11.62–14.66 respectively which are consistent with the crystallite sizes evaluated from XRD and also there is an influence of the increase in ZnO concentration on the particle sizes.

FT-IR Spectroscopy

FT-IR spectra of CdO–$FePO_4$ nanocomposites doped with ZnO recorded in the middle infrared (IR) range of 4000 to 400 cm^{-1} are shown in Fig. 7, which confirms the synchronization environments of CdO, $FePO_4$, and ZnO groups. The characteristic CdO metallic bonding appears at 470 cm^{-1} as a weak band.[24] The band at 634 cm^{-1} refers to the symmetric stretching mode of P-O. The band appearing at 1062 cm^{-1} is due to intramolecular anti-symmetric stretching vibrations of the PO_4^{3-} group.[2,25] The two higher wavenumber bands 1431 cm^{-1} and 2925 cm^{-1} are attributed to the bending vibrational mode of CH_2 molecules and CH aliphatic stretching respectively.[26] The bands at 1631 cm^{-1} and 3424 cm^{-1} are ascribed to bending and stretching vibrational modes of hydroxyl groups.[2] The band locations shift to smaller wavenumbers to a small extent with increasing ZnO content. The consequent frequencies of different peak positions in IR spectra of CdO–$FePO_4$ nanocomposites doped with ZnO are specified in Table IV. It is evident from Table IV that there is a redshift (i.e., the spectral lines move to longer wavelengths) by increasing the dopant ion concentration. This redshift could be due to the CdO–

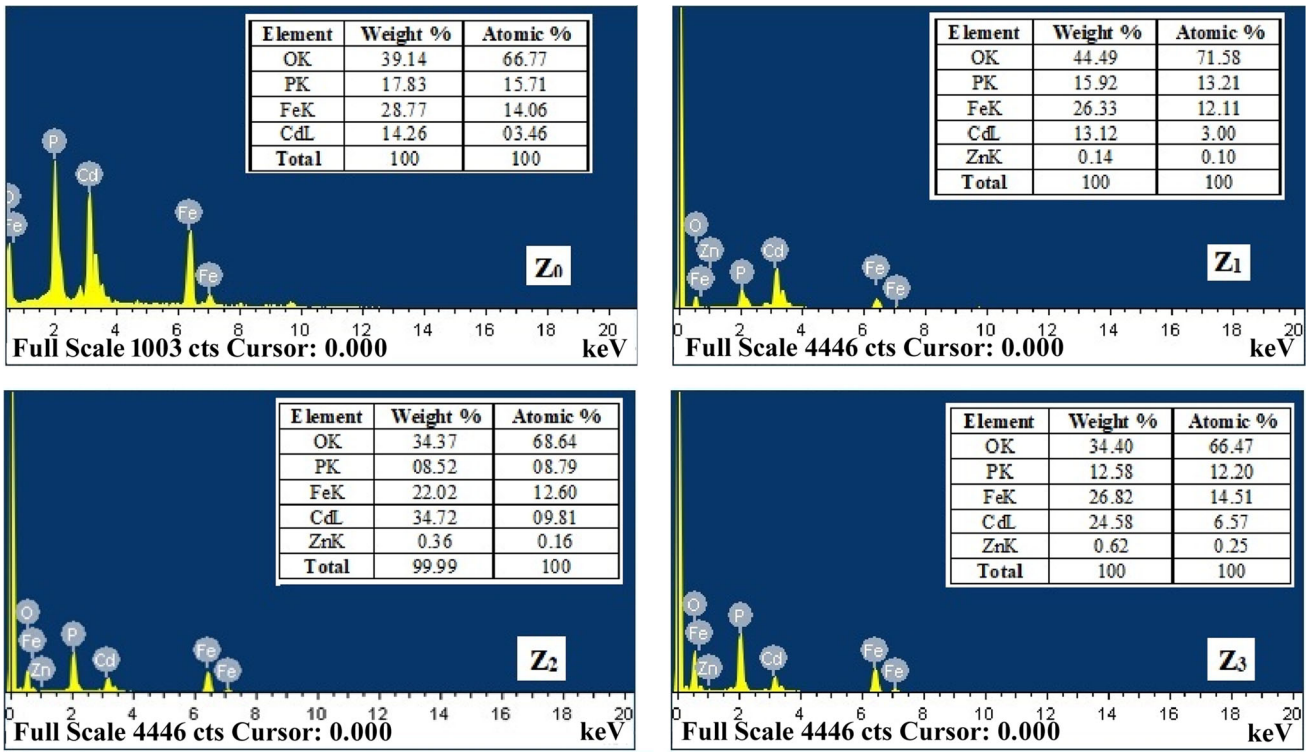

Fig 3. EDAX spectra of CdO–$FePO_4$ nanocomposites doped with ZnO.

$FePO_4$ nanostructure change, morphology, and surface microstructure. The presence of impurities relating to the C–H group may have originated from the starting precursor. This can be avoided by further annealing or improving the cleaning process.[27] The influence of environmental factors, i.e., temperature and concentration cause the positional fluctuation of peaks of IR spectra. The peak position change may be caused by the actual frequency shift of a single absorption band or alternatively by the relative intensity changes of overlapped bands or changes in bond length. The literature proposes that the shift in the peak of FT-IR spectra results from the changes in the strength of hydrogen bonds. Further, the frequency shift of –OH stretching under temperature or concentration change may be attributed to the gradual weakening of such interactions and thus results in the frequency of the band shift.[28–30]

Raman Spectroscopic Studies

Figure 8 depicts the Raman spectra of CdO–$FePO_4$ nanocomposites doped with ZnO. The Raman peak observed at 3177 cm^{-1} is due to O–H stretching vibrations.[31,32] The peak at 2125 cm^{-1} may be ascribed to the bending of the O–H…O bond.[32] The peaks at 1967, 1782 and 1602 cm^{-1} are most likely due to C=O stretching and C–C stretching, respectively.[26] For both IR and Raman spectra, the bending vibrations for CH_2 and CH_3 groups are observed in the spectral region between 1450 and 1300 cm^{-1}. Here the peak at 1474 cm^{-1} in Raman spectra and 1431 cm^{-1} in IR spectra is certainly due to the bending mode of CH_2 molecules, while the peak at 1389 cm^{-1} is most likely due to the bending of the anti-symmetric mode of CH_3 molecules.[26] The peak at 1050 cm^{-1} is ascribed to the anti-symmetric stretching vibrations of the PO_4 group.[32] Sharp and broadband peak is detected at 267 cm^{-1} which is spanned from 150–500 cm^{-1}. The other two weak peaks are also detected at 797 cm^{-1} and 900 cm^{-1}. In addition to these, another shoulder peak at 341 cm^{-1} of the major peak of 267 cm^{-1}. All four peaks occur due to the stress induced by nanostructure surface effects and are assigned to transverse and longitudinal optical modes (i.e., TO and LO) of cubic phase CdO nanostructures.[33–35] It is also observed that by increasing the dopant concentration the intensity of some Raman bands decreases and some bands disappear. The tentative assignments of Raman bands in the spectral region of 50–4000 cm^{-1} are given in Table V.

Optical Absorption Spectroscopy

The analysis of optical absorption spectra offers a very useful model to investigate optically induced electronic transitions.[36] The optical absorption spectra of CdO–$FePO_4$ nanocomposites doped with ZnO recorded in the wavelength region of 200–1200 nm at room temperature is shown in Fig. 9. The absorption bands corresponding to the undoped sample are not attained. The absorption behavior of ZnO dominated on the valence band to conduction band transition. ZnO has a good light absorption

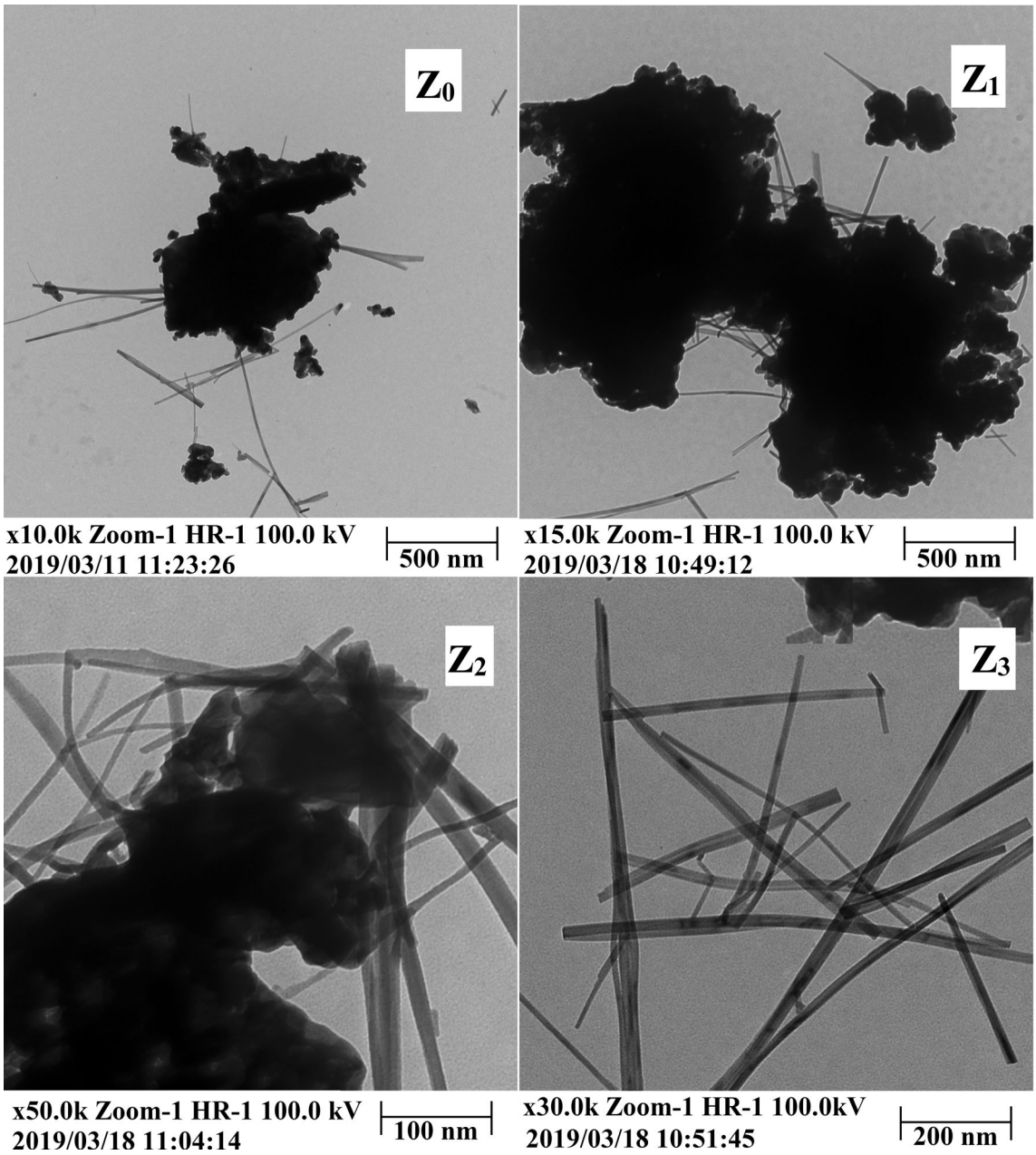

Fig 4. TEM images of CdO–$FePO_4$ nanocomposites doped with ZnO.

nature in the wavelength range of 220–350 nm.[37] The single broadband absorption is obtained for synthesized CdO–$FePO_4$ nanocomposites doped with ZnO, i.e., around 345 nm.[38]

Diffused Reflectance Spectroscopy

The optical absorption technique on diffused reflectance is used to obtain the accurate value of the optical bandgap of CdO–$FePO_4$ nanocomposites doped with ZnO. The diffused reflectance spectra of CdO–$FePO_4$ nanocomposites doped with ZnO are shown in the inset of Fig. 10. Kubelka-Munk function is applied in order to convert the reflectance values to absorbance. In general, Kubelka-Munk's theory is applied for analyses of the diffuse reflectance spectra of weakly absorbing samples. Kubelka-Munk (K–M) relation is expressed as[39–42]

$$F(R) = \frac{(1-R)^2}{2R} \tag{4}$$

where R is the diffused reflectance, $F(R)$ is K-M function related to absorbance, the relation transforming $F(R)$ value to the linear absorption coefficient is as follows[39,42,43]

$$\alpha = \frac{F(R)}{t} = \frac{\text{Absorbance}}{t} \tag{5}$$

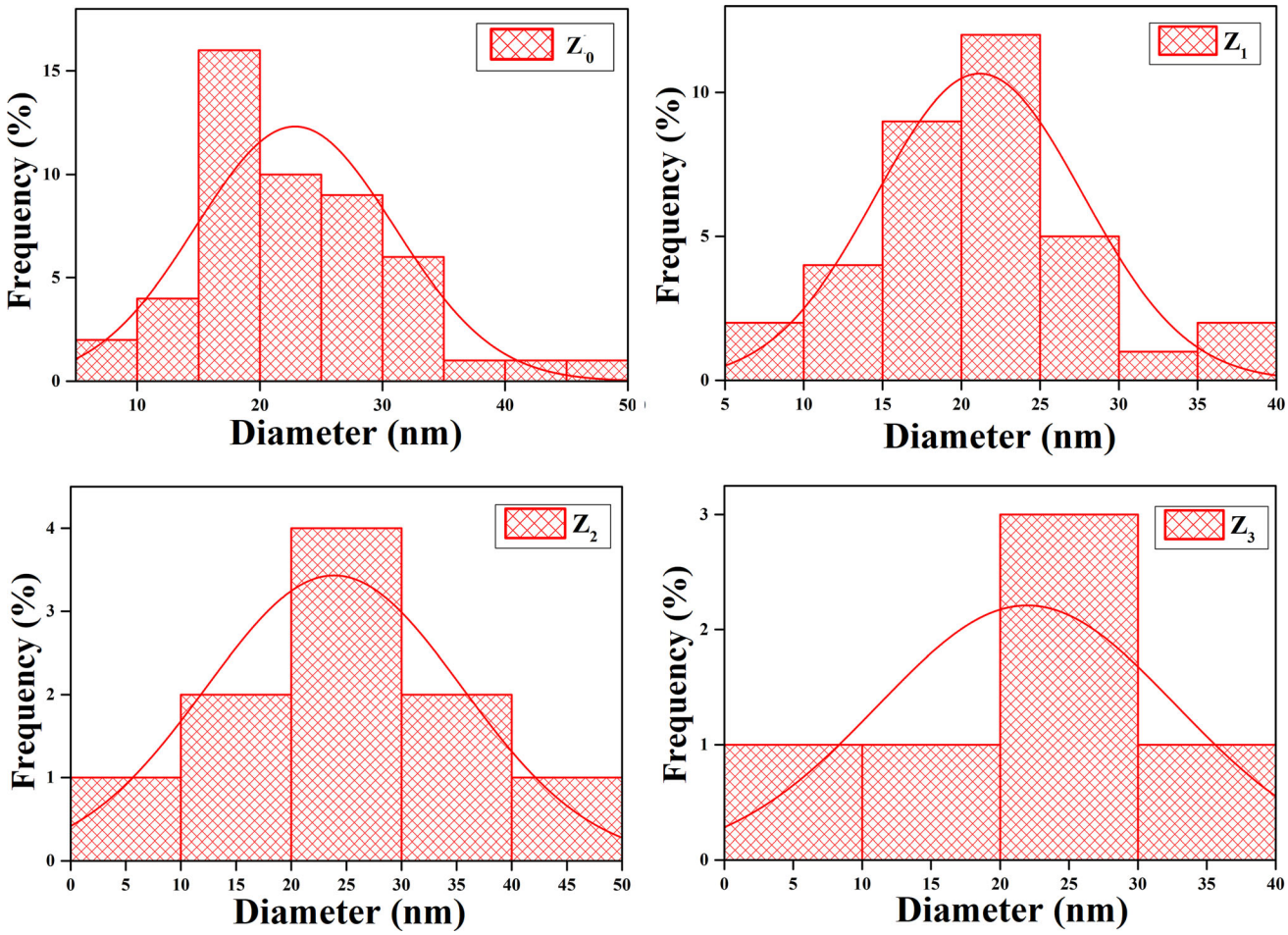

Fig 5. Particle size distribution of spherical agglomerations (nm) in CdO–$FePO_4$ nanocomposites doped with ZnO.

The equation relating absorption coefficient (α) and bandgap (E_g) is

$$(\alpha h) = A(h - E_g)^n \quad (6)$$

This equation can be rewritten as

$$(\alpha h) = F(R)h = A(h - E_g)^n \quad (7)$$

where $h\upsilon$ is the incident photon energy, A is transition probability reliant constant, n depends on transition type (i.e., 2 for indirect and 1/2 for direct allowed transitions). The plot of $(F(R)h\upsilon)^2$ versus photon energy is shown in Fig. 10. The optical bandgap values for CdO–$FePO_4$ nanocomposites doped with ZnO are obtained by extrapolating to the linear segments of these plots to the x-axis (photon energy). The bandgap values E_g obtained for CdO–$FePO_4$ nanocomposites doped with ZnO are given in Table VI. It is apparent that the optical bandgaps of the prepared nanocomposites are decreased for high dopant concentrations. The decrease of optical bandgap could be caused by the existence of intrinsic crystal defects and quantum confinement effects.[44] The optical bandgaps of the studied CdO–$FePO_4$ nanocomposites doped with ZnO are close to the results published on Fe-doped CdO nanopowders.[4] There is no existing data so far about the diffused reflectance calculations for bandgaps of CdO–$FePO_4$ nanocomposites doped with ZnO. Thus, from the obtained results of optical bandgaps, it may be considered that the as-synthesized CdO–$FePO_4$ nanocomposites doped with ZnO are promising semiconducting materials.

PL Studies

The PL spectra of CdO–$FePO_4$ nanocomposites doped with ZnO excited at a wavelength of 350 nm are shown in Fig. 11. PL intensity in the visible range can be directly related to the defect density within a nanomaterial. For CdO–$FePO_4$ nanocomposites doped with ZnO five emission peaks appear at 382 nm, 390 nm, 402 nm, 430 nm, 455 nm. No significant transformation in the intensity of the peaks is observed upon increasing dopant ion concentration. The small peak near 455 nm can be attributed to the intrinsic defects viz., interstitial defects particularly. In the case of CdO based nanocomposites, the occurrence of PL spectra in the visible range is ascribed to structural defects

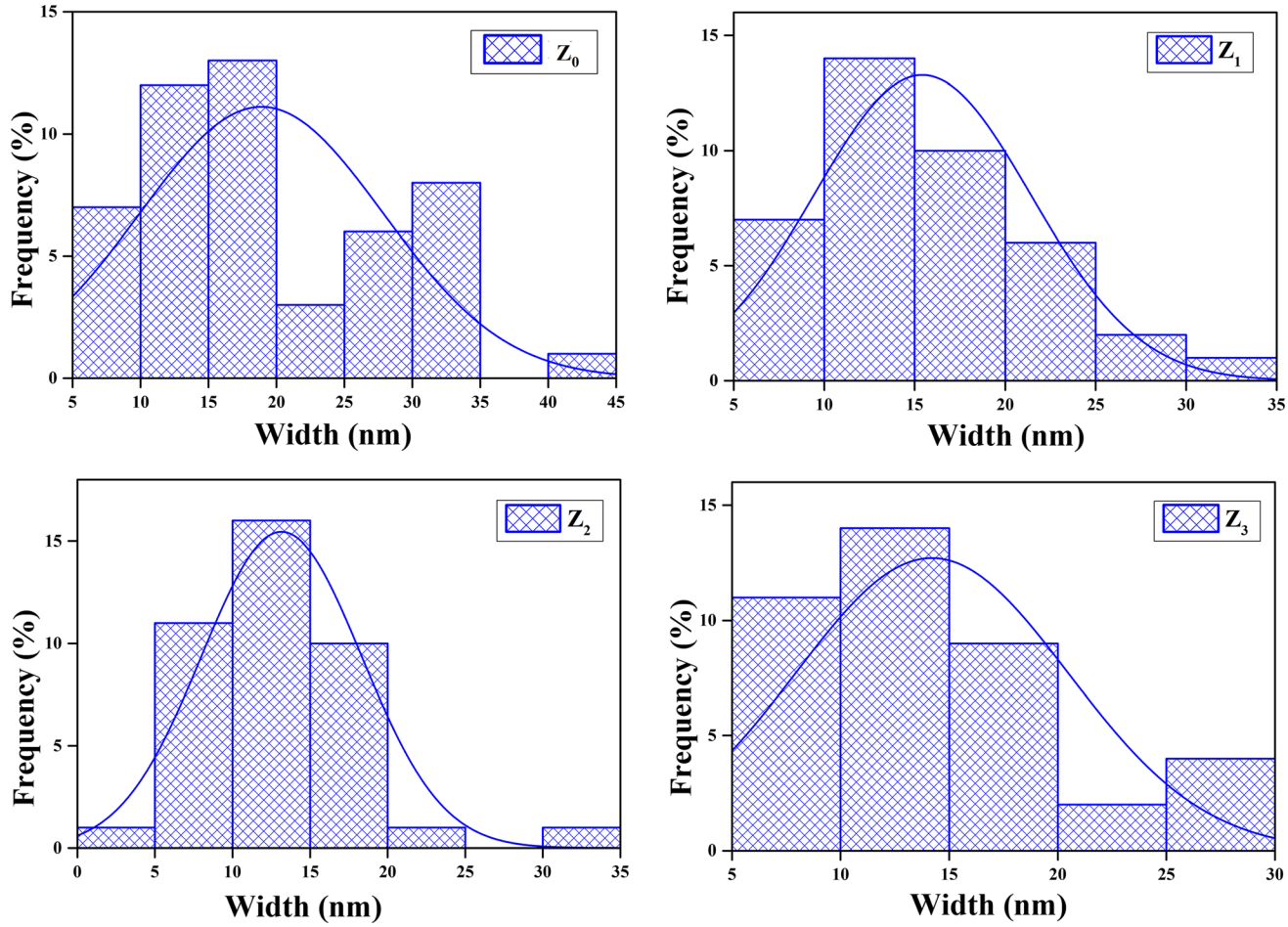

Fig 6. Particle size distribution of rods (nm) in CdO–$FePO_4$ nanocomposites doped with ZnO.

Table III. Average particle size of spherical agglomerations and rods (nm) obtained from TEM images of CdO–$FePO_4$ nanocomposites doped with ZnO

Sample code	Average particle size of spherical agglomerations (nm)	Average particle size of rods (nm)
Z_0	21.04	14.66
Z_1	20.97	13.90
Z_2	25.00	12.29
Z_3	24.70	11.625

(vacancies and surface traps).[45] The existence of Fe^{3+} ions in the lattice site can lead to the distinct excitonic emissions in the 355–430 nm range.[46] Hence, the high intensity and low intensity peaks at 430 nm and 390 nm, respectively, are ascribed to the Fe^{3+} ion. The violet emission is due to the peak at 402 nm. The peak at 382 nm could be ascribed to near band edge emission.[45] The sharp and high intensity near band edge is observed when the oxygen vacancy concentration in the prepared nanocomposites is reduced.[47] The sharp emission near the band edge in the present study confirms that the prepared samples exhibit fine optical properties having few structural defects. No significant transformation in the intensity of the peaks and shift in peak position is observed upon increasing dopant ion concentration. The slight shift of spectral lines might indicate the occurrence of quantum-confined electronic behavior.

Furthermore CIE (Commission Internationale de l'Eclairage) 1931 Chromaticity coordinates are also considered from the emission spectrum for understanding luminescent properties of the as-synthesized nanocomposites. The two-color coordinates x and y present a point in the chromaticity diagram that illustrates the colors of the CIE system. This system offers more accuracy in color measurement since the parameters depend on the spectral power

distribution (SPD) of the light emitted from a colored object. The color coordinates of CdO–$FePO_4$ nanocomposites doped with ZnO are located in the CIE chromaticity diagram are shown in Fig. 12. From this figure, it can be observed that the colors of the prepared nanocomposites are located in the blue region and the successive CIE coordinates are x =0.165, y = 0.072 for undoped and x = 0.163, 0.165 and 0.161 y = 0.079, 0.078 and 0.075 for CdO–$FePO_4$ nanocomposites doped with ZnO (0.3, 0.6, 0.9 mol.%), respectively. The quality of emitted light is estimated by calculating the CCT (color correlated temperature) values using Mc Camy's approximation[48] given by

$$CCT = -437n^3 + 3601n^2 - 6861n + 5517 \quad (8)$$

where $n = \frac{x-x_e}{y-y_e}$ is the inverse slope line. Here x_e and y_e=0.332 and 0.1858, respectively. The calculated values of CIE chromaticity coordinates and *CCT* of CdO–$FePO_4$ nanocomposites doped with ZnO from their corresponding emission spectra are incorporated in Fig. 12. The evaluated *CCT* values are found to vary from 1822 K to 1945 K. The *CCT* < 5000 K thus indicates warm white light utilized for home appliances.[49,50]

EPR Studies

To understand precisely the presence of paramagnetic defects in synthesized CdO–$FePO_4$ nanocomposites doped with ZnO, the EPR studies are carried out at room temperature. The comparisons among the EPR responses of synthesized nanocomposites for different concentrations of ZnO are conducted. The first-order differential EPR spectra of the CdO–$FePO_4$ nanocomposites doped with ZnO are presented in Fig. 13. The EPR signal is thus an indication of magnetic clustering. In general, a signal characteristic of a gyromagnetic factor g = 2 is expected for uncorrelated magnetic clusters. At the frequency operated in the works, such a signal is centered at H = 330 mT. The signal detected in the present work of CdO–$FePO_4$ nanocomposites doped with ZnO is previously detected in other $LiFePO_4$ samples containing

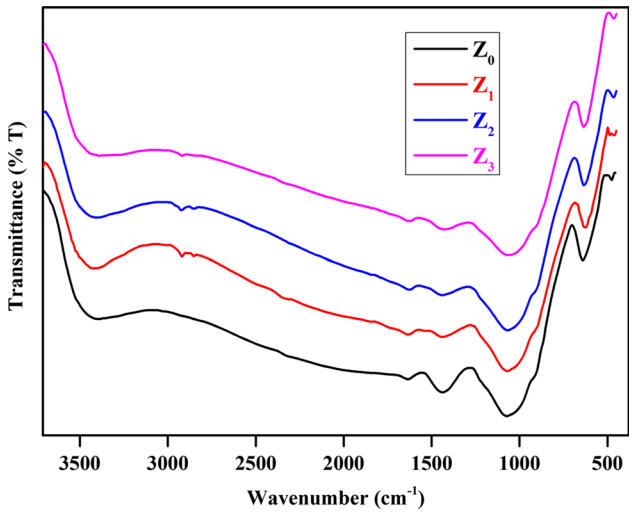

Fig 7. FT-IR spectra of CdO–$FePO_4$ nanocomposites doped with ZnO.

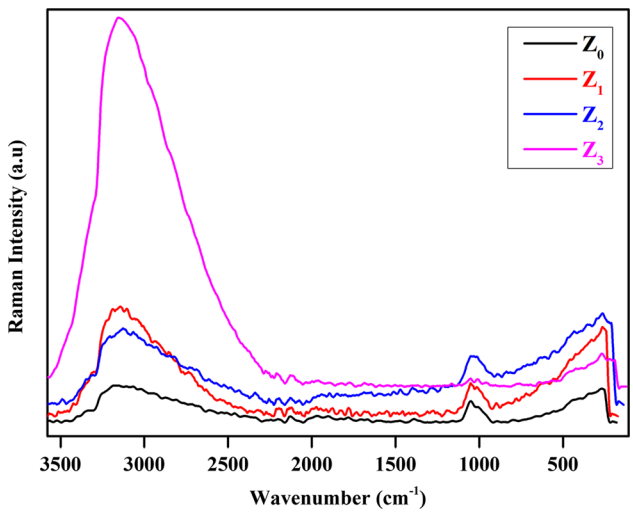

Fig 8. Raman spectra of CdO–$FePO_4$ nanocomposites doped with ZnO.

Table IV. Assignment of various peak positions and their corresponding frequencies in IR spectra of CdO–$FePO_4$ nanocomposites doped with ZnO

Wavenumber (cm^{-1})				
Z_0	Z_1	Z_2	Z_3	Assignment
3424	3416	3410	3400	–OH stretching
–	2925	2922	2920	–CH stretching
1631	1628	1626	1626	–OH bending
1431	1431	1429	1429	$–CH_2$ bending
1062	1060	1058	1058	Anti-symmetric stretching of PO_4^{3-}
634	632	628	628	Symmetric P–O stretching
470	468	464	462	Metallic bonding of CdO

Table V. Assignment of various peak positions and their corresponding frequencies in Raman spectra of CdO–$FePO_4$ nanocomposites doped with ZnO

Raman Shift (cm^{-1})				
Z_0	Z_1	Z_2	Z_3	Assignments
3177	3126	3126	3112	–OH stretching
2126	2109	2128	2132	O–H…O bond
1967	1911	–	–	C=O stretching
1782	1794			
1602	1600	–	–	C–C stretching
1474	1404	1471	–	CH_2 bending
1389	–	1398	–	CH_3 bending
1052	1050	1050	1050	Anti-symmetric stretching of PO_4 group
900	903	906	–	Metallic bonding of CdO
797	–	–	–	
341	338	341	–	
267	261	263	260	

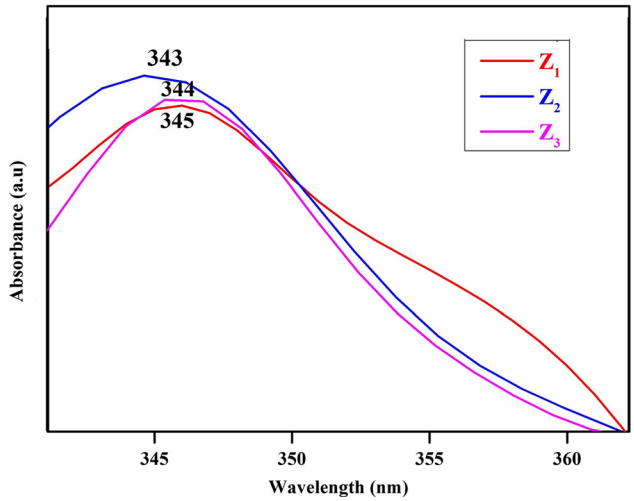

Fig 9. Optical absorption spectra of CdO–$FePO_4$ nanocomposites doped with ZnO.

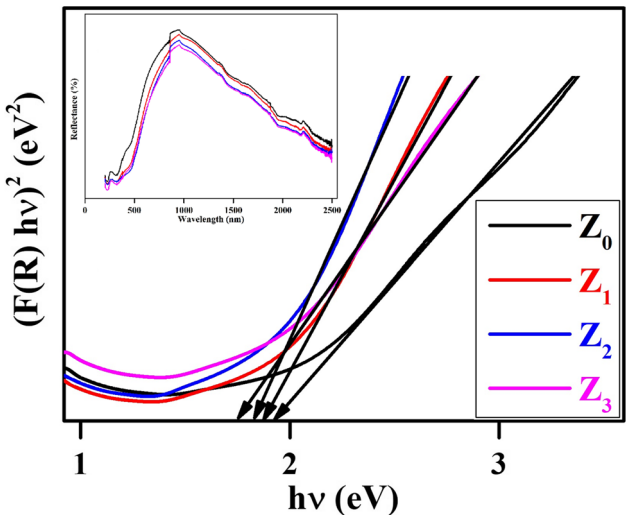

Fig 10. Plotting of $(F(R)h\upsilon)^2$ as a function of the *hv* for CdO–$FePO_4$ nanocomposites doped with ZnO. The inset is the diffused reflectance spectra of CdO–$FePO_4$ nanocomposites doped with ZnO.

ferrimagnetic particles[51,52] and is of comparable shape. The structure at 330 mT has the same width. The signal may occur not only due to ferrimagnetic clusters but also due to some defects, like an unpaired electron spin related to an oxygen vacancy or a defect due to Fe^{3+} ion. This type of defect is most susceptible to its local neighborhood that may describe the large broadening of the EPR line.

CONCLUSION

CdO–$FePO_4$ nanocomposites doped with ZnO have been successfully produced by a sol-gel approach at room temperature. The XRD analysis reveals that the prepared nanocomposites belong to a cubic system (CdO) and hexagonal system ($FePO_4$). SEM analysis showed a morphological transformation on increasing dopant concentration from spherical-like agglomerations to multi-nanorods forming networks with spherical agglomerations of ZnO doped CdO–$FePO_4$ nanostructures.

Table VI. Energy bandgap values of CdO–$FePO_4$ nanocomposites doped with ZnO

Sample code	Energy bandgap value (E_g) eV
Z_0	1.96
Z_1	1.88
Z_2	1.82
Z_3	1.75

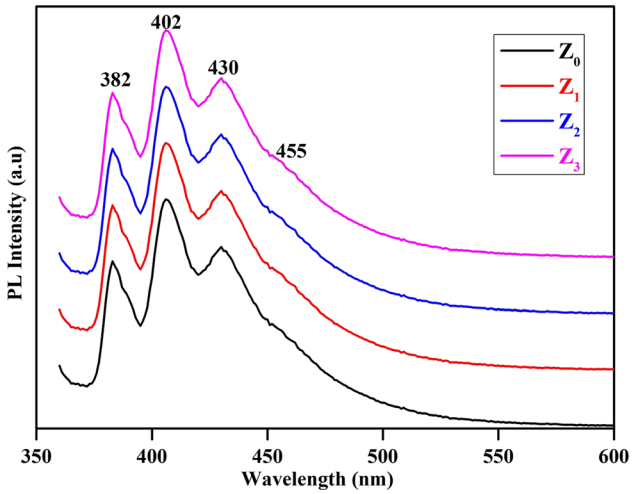

Fig 11. PL spectra of CdO–$FePO_4$ nanocomposites doped with ZnO.

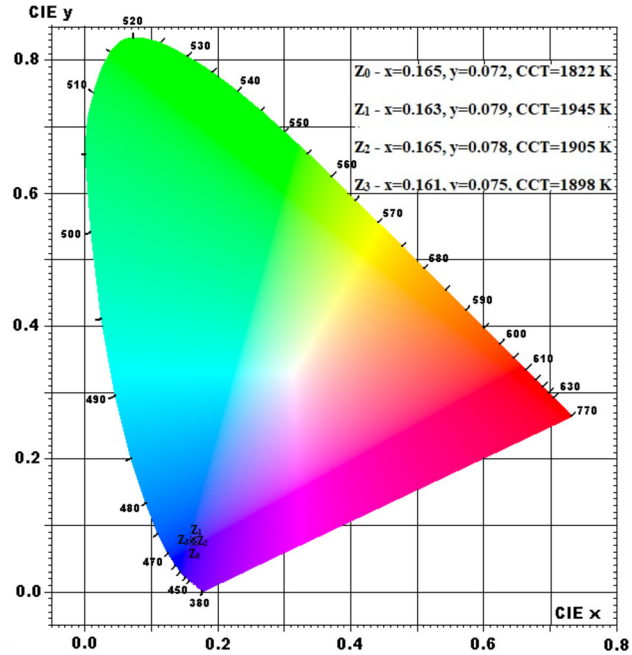

Fig 12. CIE chromaticity diagram of CdO–$FePO_4$ nanocomposites doped with ZnO.

The band positions in FT-IR spectra signify the existence of phosphate (PO_4^{3-}) groups in the prepared nanocomposites. The Raman bands in the recorded Raman spectra of the synthesized nanocomposites show a slight variation in frequencies. Optical absorption spectra show the characteristic band of Zn^{2+} ions in octahedral site symmetry. From the diffused reflection spectra, optical band-gap energies are evaluated. PL spectrum shows the enhanced blue emission of CdO–$FePO_4$ nanocomposites doped with ZnO. EPR spectra indicate the presence of ferrimagnetic clusters in the synthesized nanocomposites. It is evaluated that the obtained nanocomposites can be worn for advanced technological applications.

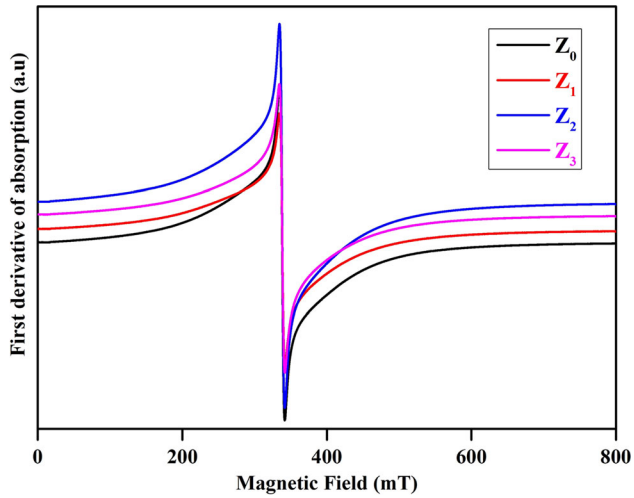

Fig 13. EPR spectra of CdO–$FePO_4$ nanocomposites doped with ZnO.

ACKNOWLEDGMENTS

One of the authors, S.K. Khaja Muswareen, expresses her heartfelt gratitude to the Acharya Nagarjuna University authorities for granting the University Research Fellowship (URF) to carry out this research work.

CONFLICT OF INTEREST

The authors declare that they have no conflict of interest.

REFERENCES

1. K. Kaviyarasu, E. Manikandan, J. Kennedy, and M. Jayachandran, *Mater. Lett.* 120, 243 (2014).
2. M. Subba Rao, K. Satyavathi, Y. Naga Bhaskararao, and C. Sandhya, *J. Alloys Compd.* 682, 7 (2016).
3. T. Aswani, V. Pushpa Manjari, B. Babu, S. Muntaz Begum, G. Rama Sundari, K. Ravindranadh, and R.V.S.S.N. Ravikumar, *J. Mol. Struct.* 1063, 178 (2014).
4. C. Aydin, O.A. AlHartomy, A.A. Al Ghamdi, F. Al Hazmi, I.S. Yahia, F. ElTantawy, and F. Yakuphanoglu, *J. Electroceram.* 29, 155 (2012).
5. P.K. Nayak, *Mater. Chem. Phys.* 112, 24 (2008).
6. Z. Tianshu, P. Hing, Z. Jiancheng, and K. Lingbing, *Mater. Chem. Phys.* 61, 192 (1999).
7. B. Lee, C. Kim, Y. Park, T.G. Kim, and B. Park, *Electrochem. Solid State Lett.* 9, E27 (2006).
8. F. Rohner, F.O. Ernst, M. Arnold, M. Hilbe, R. Biebinger, F. Ehrensperger, S.E. Pratsinis, W. Langhans, R.F. Hurrell, and M.B. Zimmermann, *J. Nutrition* 137, 614 (2007).
9. F. Zhou, K. Kang, T. Maxisch, G. Ceder, and D. Morgan, *Solid State Comm.* 132, 181 (2004).
10. M.K. Kinyanjui, P. Axmann, M. WohlfahrtMehrens, P. Moreau, F. Boucher, and U. Kaiser, *J. Phys.: Condens. Matter* 22, 275501 (2010).
11. C. Gerbaldi, G. Meligrana, S. Bodoardo, A. Tuel, and N. Penazzi, *J. Pow. Sour.* 174, 501 (2007).
12. W. Peng, L. Jiao, H. Gao, Z. Qi, Q. Wang, D. Hongmei, Y. Si, Y. Wang, and H. Yuan, *J. Pow. Sour.* 196, 2841 (2011).
13. L. Chen, W. Ping, K. Xie, J. Li, X. Bin, Yu Gaoping Cao, Y.T. Chen, Y. Zhou, L. Tianhong, and Y. Yang, *Electrochim. Acta* 92, 433 (2013).
14. K. Satyavathi, M. Subba Rao, and C. Sandhya, *J. Phys. Chem. Solids* 112, 200 (2018).
15. G. GirishKumar and S. Sampath, *Solid State Ionics* 160, 289 (2003).

16. Y. Li, M. Gong, Y. Liang, J. Feng, J.E. Kim, H. Wang, G. Hong, B. Zang, and H. Dai, *Nat. Commun.* 4, 1 (2013).
17. J. Nouri, T. Khoshravesh, S. Khanahmadzadeh, A. Salehabadi, and M. Enhessari, *Int. J. Nano Dimens.* 7, 15 (2016).
18. C. Kim, B. Lee, Y. Park, and B. Park, *Appl. Phys. Lett.* 91, 113101 (2007).
19. H.C. Liu, W.H. Ho, C.F. Li, and S.K. Yen, *J. Electrochem. Soc.* 155, E178 (2008).
20. Y. Song, S. Yang, P.Y. Zavalij, and M.S. Whittingham, *Mater. Res. Bull.* 37, 1249 (2002).
21. C.S. Tiwary, R. Sarkar, P. Kumbhar, and A.K. Mitra, *Phys. Lett. A* 372, 5825 (2008).
22. A.R. Stokes and A.J.C. Wilson, *Proc. Phy. Society* 56, 174 (1944).
23. G. Tirumala Rao, B. Babu, R. JoyceStella, V. PushpaManjari, C. VenkataReddy, J. Shim, and R.V.S.S.N. Ravikumar, *J. Mol. Struct.* 1081, 254 (2015).
24. R. Joyce Stella, G. Thirumala Rao, V. Pushpa Manjari, B. Babu, C. Rama Krishna, and R.V.S.S.N. Ravikumar, *J. Alloys Compd.* 628, 39 (2015).
25. Y. Naga Bhaskararao, K. Satyavathi, M. Subba Rao, and C. Sandhya, *J. Mol. Struct.* 1130, 585 (2017).
26. B.M. Sukarova, B. Mangovska, G.B. Gaceva, and V.M. Petrusevskia, *Croat. Chem. Acta* 85, 63 (2012).
27. M.M. Ba-Abbad, A.A.H. Kadhum, A.B. Mohamad, M.S. Takriff, and K. Sopian, *J. Alloy. Compd.* 550, 63 (2013).
28. A. Ananth, S. Dharaneedharan, M.-S. Heo, and Y.S. Mok, *Chem. Eng. J.* 262, 179 (2015).
29. S.R. Ryu, I. Noda, and Y.M. Jung, *Bull. Korean Chem. Soc.* 32, 4011 (2011).
30. H. Mersiana, M. Alizadeh, and N. Hadi, *Ceram. Int.* 44, 20399 (2018).
31. D. Kang, X. Wu, G. Yuan, S.X. Huang, J.J. Niu, J. Gao, and S. Qin, *Chin. Phys. B* 27, 017402 (2018).
32. H. Zho, F. Wang, M. Xu, B. Liu, F. Liu, L. Zhang, X. Xu, X. Sun, and Z. Wang, *J. Cryst. Growth* 450, 6 (2016).
33. K. Sirohi, S. Kumar, V. Singh, and A. Vohra, *Acta Metall. Sin. Engl. Lett.* 31, 254 (2018).
34. F.T. Thema, P. Beukes, A.G. Fakim, and M. Maaza, *J. Alloys Compd.* 646, 1043 (2015).
35. S. Kumar, A.K. Ojha, and B. Walkenfort, *J. Photochem. Photobiol.* 159, 111 (2016).
36. M. Altaf, M.A. Chaudhry, and Z. Maria, *J. Res. Sci.* 14, 253 (2003).
37. S.J. Chen, Y.C. Liu, J.G. Ma, Y.M. Lu, J.Y. Zhang, D.Z. Shen, and X.W. Fan, *J. Cryst. Growth* 254, 86 (2003).
38. O. Slimi, D. Djouadi, L. Hammaiche, A. Chelouche, and T. Touam, *J. Porous Mater.* 25, 595 (2018).
39. A. EscobedoMorales, E. SanchezMora, and U. Pal, *Rev. Mex. Fis. S* 53, 18 (2007).
40. V. Senthilkumar, P. Vickraman, and R. Ravikumar, *J. Sol-Gel. Sci. Technol.* 53, 316 (2010).
41. F. Yakuphanoglu, *J. Alloys Compd.* 507, 184 (2010).
42. F. Yakuphanoglu, R. Mehrotra, A. Gupta, and M. Munoz, *J. Appl. Polymer Sci.* 114, 794 (2009).
43. E. Yassitepe, Z. Khalifa, G.H. Jaffari, C.S. Chou, S. Zulfiqar, M.I. Sarwar, and S.I. Shah, *Powder Technol.* 201, 27 (2010).
44. M. Pudukudy and Z. Yaakob, *J. Clust. Sci.* 26, 1187 (2015).
45. T. Aswani, B. Babu, V. Pushpa Manjari, R. Joyce Stella, G. Thirumala Rao, C. Rama Krishna, and R.V. Ravi kumar, *Spectrochim. Acta A Mol. Biomol. Spectrosc.* 121, 544 (2014).
46. P.B. Nair, V.B. Justinvictor, G.P. Daniel, K. Joy, V. Ramakrishnan, D.D. Kumar, and P.V. Thomas, *Thin Solid Films* 550, 121 (2014).
47. D. Ying, Y. Zhang, Y.D. Bai, and Z.L. Wang, *Chem. Phys. Lett.* 375, 96 (2003).
48. C.S. McCamy, *Color. Res. Appl.* 17, 142 (1992).
49. C. VenkataReddy, C. RamaKrishna, T. RaghavendraRao, U.S. Udayachandran, T.Y.P. Reddy, P.S. Rao, and R.V.V.S.N. Ravikumar, *J. Mol. Struct.* 1012, 17 (2012).
50. K. Srinivasulu, I. Omkaram, H. Obeid, A. Suresh Kumar, and J.L. Rao, *J. Alloys Compd.* 546, 208 (2013).
51. A.A. Salah, A. Mauger, C.M. Julien, and F. Gendron, *Mater. Sci. Eng., B* 129, 232 (2006).
52. A.A. Salaha, J. Dodd, A. Mauger, R. Yazami, F. Gendron, C.M. Julien, and Z. Anorg, *Allg. Chem.* 632, 1598 (2006).